Journal: ***Journal of Membrane Science***

Title: Characterization of CO_2 Flux Through Hollow-Fiber Membranes Using pH Modeling

Tarun Shesh[1,2], Everett Eustance[1,*], Yen-Jung Sean Lai[1], Bruce E. Rittmann[1]

[1]Biodesign Swette Center for Environmental Biotechnology, Arizona State University, Tempe, AZ, 85287

[1]School for Engineering of Matter, Transport and Energy, Arizona State University, Tempe, AZ, 85287

[*]Corresponding Author

Everett Eustance

Email: everett.eustance@asu.edu

Phone: 1-480-727-0434

Highlights:

- A model was used to compute CO_2-transfer kinetics from real-time pH measurements
- CO_2-delivery kinetics for bubbleless gas-transfer membranes was assessed
- CO_2 flux increased approximately linearly with partial pressure in open-end mode
- Relationship of CO_2 flux to CO_2 partial pressure was non-linear for closed-end mode
- While K_L is constant, K_La decreased due to CO_2 depletion in closed-end mode

Abstract:

CO_2 must be delivered efficiently during large-scale microalgal cultivation. Bubbleless mass-transfer via diffusion through hollow-fiber membranes (HFM) can achieve much higher CO_2-transfer efficiency than traditional sparging systems. This study developed and used a model to compute accurate values for the CO_2 flux (J_{CO2}), overall mass-transfer coefficient (K_L), and overall volumetric mass-transfer coefficient (K_La) based on the rate of change of pH in batch experiments. A composite HFM comprised of two macroporous polyethylene layers and a nonporous polyurethane layer was tested for CO_2 transfer to a sodium carbonate solution using a range of total pressures, inlet CO_2 concentrations, and open-end versus closed-end modes of operation. The model accurately computed J_{CO2} and K_La for pH values above 8. Key trends are that (i) J_{CO2} and K_La increased with increasing average inlet CO_2 partial pressure; (ii) open-end HFMs performed better than closed-end HFMs when the supplied CO_2 was less than 100%; and (iii) the available membrane area used for CO_2 mass-transfer decreased as the inlet CO_2 partial pressure decreased due to depletion of CO_2 inside the membrane, especially for closed-end HFMs, since inert gases could not be vented.

Keywords: CO_2 delivery; Membrane carbonation; Hollow fiber membrane; Mathematical modelling

Nomenclature

a – Gas-liquid interfacial area per unit volume (m^{-1})

$[Alk]_0$ – Alkalinity at t = 0 (mol L^{-1})

ΔC – Driving force for CO_2 transfer

$C_{CO_{2(aq)}}$ – CO_2 concentration in bulk liquid phase (mol L^{-1})

$C^*_{CO_{2(aq)}}$ – Liquid-phase equilibrium concentration of CO_2 with gas phase (mol L^{-1})

C_T – Dissolved inorganic carbon concentration (mol L^{-1})

$C_{T,0}$ – Dissolved inorganic carbon concentration at t = 0 (mol L^{-1})

D – Membrane diameter (m)

H^{cp} – Henry's law constant ($mol_{gas}\ L_{soln}^{-1}\ atm^{-1}$)

H^{cp*} - Effective Henry's law constant ($mol_{gas}\ L_{soln}^{-1}\ atm^{-1}$)

J_{CO_2} – CO_2 flux (g m^{-2} min^{-1})

K_L – Overall mass-transfer coefficient (m/hr)

K_La – Overall volumetric mass-transfer coefficient (hr^{-1})

K – Hydration equilibrium constant

K_1 – First acid dissociation equilibrium constant

K_2 – Second acid dissociation equilibrium constant

K_w – Ionic product of water dissociation

l – Membrane length (m)

m_{CO_2} – Mass of CO_2 in solution (g)

MW_{CO_2} – Molar mass of CO_2 (g mol^{-1})

N_{CO_2} – CO_2 flux (mol m^{-3} min^{-1})

P – Total gas pressure (kPa)

P_{CO_2} – Partial pressure of CO_2 (kPa)

SA – Mass-transfer surface area (m^2)

t – Time (min)

V – Reactor volume (L)

[x] – Concentration of species x (mol L^{-1})

Greek Symbols

α_0 – Ionization fraction of the equilibrium mixture, $H_2CO_3^*$

α_1 – Ionization fraction of bicarbonate, HCO_3^-

α_2 – Ionization fraction of carbonate, CO_3^{2-}

1. Introduction

The cost of carbon dioxide (CO_2) delivery is an important factor in techno-economic assessments for large-scale cultivation of microalgae. Because the cost of CO_2 can vary from \$40 to \$230 per metric ton, CO_2 must be delivered efficiently [1–3]. One promising method to achieve nearly 100% CO_2-transfer efficiency is using hollow-fiber gas-transfer membranes [4]. CO_2 diffuses through the walls of the bubbleless membranes based on a concentration gradient caused by CO_2 uptake in the liquid medium. The rate of CO_2 delivery depends on the CO_2 concentration in the supplied gas, its concentration in the medium, and properties of the membrane wall.

Highly permeable silicone-rubber membranes were evaluated in the past, but are expensive and have thick walls that increase mass-transfer resistance [5]. Microporous polypropylene (PP) also was attempted, but the gas pressure has to be maintained in a narrow range to avoid bubble formation or water intrusion into the lumen [6]. The addition of a nonporous layer, for example polydimethylsiloxane (PDMS) coated PP fibers, prevents bubble formation allowing for high internal gas pressures [7], but PDMS-coated fibers are expensive [7]. Mitsubishi-Rayon Co. (Japan) manufactures composite hollow-fiber membranes (HFM) with a nonporous polyurethane core (1-µm thick) surrounded by two macroporous polyethylene layers. The dense polyurethane core allows bubbleless gas transfer over a wide range of lumen pressures, which offsets any gas-transfer resistance of the nonporous layers [8,9]. Using bubbleless gas-transfer of CO_2, called membrane carbonation (MC), allows precise control of the CO_2-delivery rate and minimal loss of CO_2 to the atmosphere [4].

No matter the membrane type, an accurate and rapid method to evaluate the flux of CO_2 delivery from the HFM into the liquid is valuable in evaluating membranes and operating

131 strategies. One method is based on the real-time measurement of pH changes as CO_2 is
132 delivered into a carbonate solution. This method takes advantage of the fact that dissolved
133 inorganic carbon (DIC) exists as several inter-convertible chemical forms based on the pH of the
134 solution: dissolved carbon dioxide ($CO_{2(aq)}$), carbonic acid (H_2CO_3), bicarbonate (HCO_3^-), and
135 carbonate (CO_3^{2-}) [10,11]. CO_2 dissolves in water to form $CO_{2(aq)}$, which is converted to H_2CO_3.
136 The sum of H_2CO_3 and $CO_{2(aq)}$ is termed $H_2CO_3^*$. When the water contains base (or alkalinity),
137 H_2CO_3* dissociates to form HCO_3^- and then CO_3^{2-} if enough base is present.
138 The concentration of gaseous CO_2 in the membrane lumen, the concentration of dissolved
139 CO_2 in the liquid, and the hydrodynamic conditions of the culture play important roles in the
140 CO_2 transfer rate. The CO_2 concentration in the inlet gas stream can range from 0.04%
141 (atmospheric CO_2 partial pressure) to 100%. However, mass transfer is limited when
142 atmospheric air is used, since the concentration of CO_2 is very low (400 ppm) [10,12].
143 Increasing the CO_2 concentration in the gas's influent stream can increase the rate of CO_2
144 transfer to the culture medium. Thus, changing the CO_2 partial pressure inside the fiber is one of
145 the factors that changes the rate of gas-transfer, permitting accurate control over CO_2 delivery
146 capacity [4,13].
147 Typically, gas is supplied through one end of the HFM fiber. An important distinction is
148 how the other end of the fiber is managed. HFMs for microalgal cultivation can be operated as
149 open-end or closed-end. The implications of each choice are profound in terms of CO_2-transfer
150 efficiency and rate.
151 In a closed-end HFM, all the CO_2 supplied to the membrane diffuses across the
152 membrane's wall into the liquid phase. Since no CO_2 exits from the far end, closed-end
153 operation allows for 100% CO_2 transfer efficiency [14]. However, when the inlet gas is not pure

CO_2, the CO_2 partial pressure in the lumen decreases along the fiber length due to the selective retention of inert gases (e.g., N_2 and O_2 in flue gas) [8,9,14,15]. In addition, inert gases in the liquid medium can diffuse into the lumen: e.g., water vapor, N_2, and O_2. The buildup of inert gases affects CO_2 transfer rates, since the distal end of the fiber lumen may become devoid of CO_2, thus reducing the average CO_2 partial pressure along the fiber length [14]. Back-diffusion of water vapor also poses a concern as condensation inside the lumen may occur and adversely affect the performance of the fibers [8].

In an open-end HFM, gas continually flows through the membrane, which minimizes the buildup of any inert gases by sweeping them out from the open end of the lumen. Thus, the CO_2-concentration can be nearly uniform along the fiber length, which means that the average CO_2 concentration does not decline due to the buildup of inert gases. The disadvantage of an open-end HFM is that CO_2-transfer efficiency is sacrificed, because CO_2 is vented out the distal end [9,14].

The first objective of this work is to develop a rapid method to quantify CO_2 transfer rates and mass-transfer coefficients for HFMs. The method is based on real-time measurement of pH changes as CO_2 is delivered into an abiotic carbonate solution. A mathematical model relates the pH change to the concentration of CO_2 delivered to the solution. The second objective is to apply the model to evaluate CO_2-delivery performance when delivering CO_2 from a broad range of sources and with closed- or open-end operation. This method of determining CO_2 fluxes is advantageous, because measuring pH is non-destructive, rapid, and inexpensive. The model can reflect the effects of CO_2 concentration in solution, as well as in the HFM lumen.

2. Materials and Methods

2.1. Experimental Setup

The experimental setup for abiotic testing is shown in Figure 1. The solution used for the experiments was 5 mM sodium carbonate prepared using deionized (DI) water and sodium carbonate powder (EMD, USA). The initial pH of the solution was ~10.8. The solution was poured into a "500-mL" glass bottle (PYREX, Germany) that had a total capacity of 700 mL when filled to the top to minimize headspace. A magnetic stir bar and stir plate (Super-Nuova, Thermo Fisher Scientific, USA), set at 600 rpm, were used to ensure well-mixed conditions inside the bottle. The glass bottle was sealed with a lid modified to have openings for a pH probe and membrane module connections to minimize gas exchange with the surrounding air. Polyurethane tubing (Surethane NSF-51, ATP, USA) was used as the connection tubing through which gas was supplied.

Various compositions of gases were used: 100% CO_2, 90% CO_2, 50% CO_2, and 10% CO_2. The balancing gas in the latter three cases was air (~79% N_2 and 21% O_2). Gas was supplied from a gas cylinder (PRAXAIR, USA) with the pressure being controlled by a regulator. Gas was supplied at 69 kPa-gauge for all experiments. The volumetric flow rate, mass flow rate, temperature, and pressure at the inlet and outlet of the system was recorded using flow meters (MC Series, ALICAT Scientific, USA). The pH of the solution was measured using a glass electrode pH meter (Lab 860 pH meter, Schott Instruments, Germany).

A composite HFM (Model MHF 200TL, Mitsubishi-Rayon Co., Ltd., Japan) that consisted of a 1 µm-thick, nonporous polyurethane inner layer sandwiched between two macroporous polyethylene layers (thickness of 40 µm and pore size of 0.1 – 0.15 µm) was used. The dense, nonporous polyurethane layer blocks any continuous pores, allowing for high

200 operating pressures in the lumen, but without bubble formation. The length of the composite
201 HFM varied from 13 to 39 cm, depending on the experiment.
202 For experiments conducted with modules consisting of 96 fibers and 64 fibers, a urethane
203 adhesive (3M Scotch-Weld 3532 B/A) was used to glue the ends of the fibers together in a piece
204 of polyethylene tubing. However, cutting fibers to a specific length can pinch or seal some of
205 the fibers, leading to their loss of gas-transfer utility. Thus, later experiments, conducted with 32
206 fibers, employed a potting method that used a liquid resin (Max Bond low viscosity industrial
207 strength adhesive) to encase the fibers prior to cutting, which eliminated pinching of fibers
208 [16,17]. The model for computing CO_2-transfer kinetics was equally valid for all HFMs,
209 regardless of potting method.
210 Experiments involved mass transfer of CO_2 to the bulk liquid. Uptake of CO_2 increased
211 the DIC and decreased the pH from the starting value of ~10.8. Experiments were conducted
212 until the pH of the solution dropped to 7. Experiments were conducted at room temperature,
213 which was 25 ± 1°C. To remove any residual gas present in the lumen of the membranes, the
214 HFM modules were flushed for about 10 minutes and pressurized with the experiment gas prior
215 to immersion in solution.
216 In experiments to verify the accuracy of the model developed to quantify the CO_2 flux
217 through the membrane module (Section 2.4), samples were taken from the sodium carbonate
218 solution at regular pH intervals to measure DIC using a total-organic-carbon analyzer (TOC-V,
219 Shimadzu Corp., Japan). 15-mL samples were taken in glass falcon tubes at pH intervals of 0.25
220 between the pH range 8 – 10. Normally, 15 mL of acidified DI water must be used to dilute the
221 samples in order to run them through the TOC-V instrument, since DI-water dilution reduces the
222 lifetime of the catalyst used in the instrument. However, acidified DI water resulted in CO_2 off-

gassing from the samples before they could be injected into the TOC instrument. Thus, samples were diluted with non-acidified DI water for a set of experiments to confirm the accuracy of DIC computations. One advantage of using the model to convert pH to DIC is that it provides flux and mass-transfer coefficient without DIC analyses. This provides accurate, real-time values for DIC while avoiding harm to the TOC-V analyzer.

Off-gassing of dissolved CO_2 from the solution occurred simultaneously with CO_2 delivery when the pH of the solution dropped below equilibrium with atmospheric CO_2, at approximately 8.8. The driving force for off-gassing became large enough to see its impact for pH less than about 7.5. To ensure that CO_2 was lost from solution was negligible, only measurements for pH $\geq$ 8 were utilized.

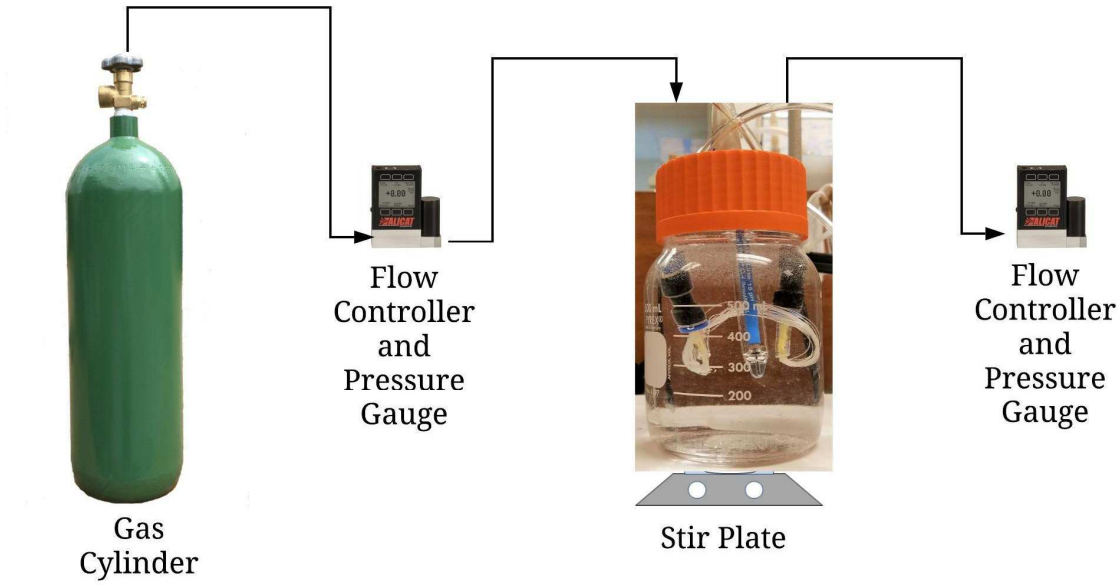

Figure 1. Experimental setup used for abiotic testing.

2.2. Mass-Transfer Theoretical Considerations

The rate at which CO_2 is transferred from the gas phase to the liquid phase (N_{CO_2}, mol m^{-3} min^{-1}) is proportional to the driving force, i.e., the concentration gradient and the mass-transfer area. This rate can be calculated by the following mass balance:

$$N_{CO_2} = \frac{dC}{dt} = K_L a \ (C^*_{CO_{2(aq)}} - C_{CO_{2(aq)}}) \quad (1)$$

where $K_L a$ (min^{-1}) is the overall volumetric mass-transfer coefficient for CO_2, K_L is the mass-transfer coefficient (m min^{-1}), a denotes the gas-liquid interfacial area per unit volume of liquid (m^{-1}), $C_{CO_{2(aq)}}$ (mol L^{-1}) is the concentration of CO_2 dissolved in the bulk liquid, and $C^*_{CO_{2(aq)}}$ (mol L^{-1}) is the liquid-phase equilibrium concentration of CO_2 with the gas phase. $K_L a$ lumps all resistances, including the lumen side, the membrane wall, and the water side [18].

2.3. Carbonate Equilibrium

When gaseous CO_2 dissolves in water, it undergoes three chemical reactions involving four chemical species, as shown in the equilibria in Eq. 2:

$$H_2O_{(l)} + CO_{2(aq)} \overset{K}{\leftrightarrow} H_2CO_{3(aq)} \overset{K_1}{\leftrightarrow} HCO^-_{3(aq)} + H^+_{(aq)} \overset{K_2}{\leftrightarrow} CO^{2-}_{3(aq)} + 2H^+_{(aq)} \quad (2)$$

The law of mass action can be applied to any of the reactions in Eq. 2, e.g.,

$$K = \frac{[H_2CO_3]}{[CO_2]} \quad (3)$$

At 25ºC, K is equal to 650 [19]. Eq. 3 can then be simplified to,

$$[CO_{2(aq)}] = 650\ [H_2CO_3] \quad (4)$$

Less than 0.3% of CO_2 reacts with water to form carbonic acid; thus, the concentration of dissolved CO_2 (i.e., $[CO_{2(aq)}]$) is much greater than that of H_2CO_3, and a large fraction of un-

ionized carbon dioxide is present in the form of $CO_{2(aq)}$ [11,19,20]. According to convention, the equilibrium mixture, $H_2CO_3^*$, is

$$[H_2CO_3^*] = [CO_{2(aq)}] + [H_2CO_3] \quad (5)$$

Due to the low concentration of H_2CO_3 compared to $CO_{2(aq)}$, substituting Eq. 5 into Eq. 4 yields

$$(0.998) \times [H_2CO_3^*] = [CO_{2(aq)}] \quad (6)$$

Similar to Eq. 3, the equilibrium constants for all the reactions shown in Eq. 2 can be defined as

$$K_1 = \frac{[H^+]\ [HCO_3^-]}{[H_2CO_3^*]} \quad (7)$$

$$K_2 = \frac{[H^+]\ [CO_3^{2-}]}{[HCO_3^-]} \quad (8)$$

The mass balance equation to compute DIC, or the sum of all the dissolved inorganic carbon species in solution, is

$$C_T = [H_2CO_3^*] + [HCO_3^-] + [CO_3^{2-}] \quad (9)$$

If no other acid or base species is present, a charge-balance or proton-condition equation is

$$[H^+] = [OH^-] + [HCO_3^-] + 2\,[CO_3^{2-}] \quad (10)$$

The ionization fractions (α values) for $H_2CO_3^*$, HCO_3^-, and CO_3^{2-} can be calculated based on Eqs. 7 – 10,

$$\alpha_0 = \alpha_{H_2CO_3^*} = \frac{[H^+]^2}{[H^+]^2 + [H^+]\,K_1 + K_1\,K_2} = \frac{[H_2CO_3^*]}{C_T} \quad (11)$$

$$\alpha_1 = \alpha_{HCO_3^-} = \frac{[H^+]\,K_1}{[H^+]^2 + [H^+]\,K_1 + K_1K_2} = \frac{[HCO_3^-]}{C_T} \quad (12)$$

$$\alpha_2 = \alpha_{CO_3^{2-}} = \frac{K_1\,K_2}{[H^+]^2 + [H^+]\,K_1 + K_1K_2} = \frac{[CO_3^{2-}]}{C_T} \quad (13)$$

where the subscript on α represents the number of protons lost from the most protonated species [11].

The driving force for carbon dioxide transfer (ΔC) is based on the measured dissolved CO_2 concentration ($C_{CO_{2(aq)}}$) and the CO_2 concentration in the liquid phase that would equilibrate the gas phase ($C^*_{CO_{2(aq)}}$). $C_{CO_{2(aq)}}$ was calculated using Eqs. 6 and 11. The partial pressure of carbon dioxide (P_{CO_2}) was computed using the composition of carbon dioxide used in the inlet stream and the pressure of the gas supplied. Eq. 14 shows that $C^*_{CO_{2(aq)}}$ can be calculated using Henry's law.

$$C^*_{CO_{2(aq)}} = H^{cp} \times P_{CO_2} = H^{cp} \times \%CO_2 \times P \tag{14}$$

where H^{cp} is the Henry's law constant.

The analytical definition of alkalinity, $[Alk]_0$, is:

$$[Alk]_0 = [HCO_3^-] + 2\,[CO_3^{2-}] + [OH^-] - [H^+] \tag{15}$$

The total alkalinity was fixed at 10 mM for all experiments.

To relate the aqueous-phase concentrations to P_{CO_2}, Eq. 14 can be substituted into Eqs. 7 and 8 to obtain:

$$[HCO_3^-] = \frac{K_1 H^{cp} P_{CO_2}}{[H^+]} \tag{16}$$

$$[CO_3^{2-}] = \frac{K_1 K_2 H^{cp} P_{CO_2}}{[H^+]^2} \tag{17}$$

Eq. 15 can then be substituted into Eq. 9 to obtain:

$$C_T = H^{cp} P_{CO_2} \left(1 + \frac{K_1}{[H^+]} + \frac{K_1 K_2}{[H^+]^2}\right) \tag{18}$$

Since more inorganic carbon is dissolved than is expected from Henry's law for $CO_{2(aq)}$ alone, the effective Henry's law constant can be defined as:

$$H^{cp*} = H^{cp} \left(1 + \frac{K_1}{[H^+]} + \frac{K_1 K_2}{[H^+]^2}\right) \tag{19}$$

300 $H^{cp*} > H^{cp}$ because the dissolved carbon dioxide can be stored in the form of bicarbonate or
301 carbonate. If the solution consisted of only $CO_{2(aq)}$, then $H^{cp*} = H^{cp}$. Since carbon speciation in
302 the solution depends heavily on pH, H^{cp*} at pH > 8 will be significantly higher than H^{cp}. At pH 8
303 and a temperature of 25°C, the value of H^{cp*} is 14.8 mol m^{-3} kPa^{-1} (1.5 mol L^{-1} atm^{-1}), while
304 the value of H^{cp} is 0.336 mol m^{-3} kPa^{-1} (0.034 mol L^{-1} atm^{-1}).
305
306 **2.4. Numerical Model for Flux and Mass-Transfer Coefficient**
307 First, the increase in the total concentration of DIC (C_T) was computed based on the total
308 alkalinity ($[Alk]_0$ = 10 mM), which was constant during an experiment, and the change in pH
309 over time due to the acidification effect of CO_2 addition. The concentration of protons in the
310 solution ($[H^+]$) was calculated based on the measured pH of the solution using Eq. 20.
311 $$[H^+] = 10^{-\mathrm{pH}} \quad (20)$$
312 and the concentration of OH^- was computed from the mass-action equation for water
313 dissociation, Eq. 21.
314 $$K_W = [H^+]\,[OH^-] \quad (21)$$
315 The ionization fractions for $H_2CO_3^*$, HCO_3^-, and CO_3^{2-} ($\alpha_{H_2CO_3^*}$, $\alpha_{HCO_3^-}$, and $\alpha_{CO_3^{2-}}$) were
316 computed from Eqs. 11 – 13. Then, C_T was then calculated using Eq. 22, which was derived by
317 rearranging the analytical definition of alkalinity and substituting Eqs. 11, 12, 13, and 21.
318 $$C_T = \frac{[Alk]_0 - \frac{K_W}{[H^+]} + [H^+]}{\alpha_1 + 2\alpha_2} \quad (22)$$
319 The mass of DIC in the media expressed in grams of carbon dioxide (m_{CO_2}) present in the
320 solution was then calculated based on C_T and the reactor volume (V), as shown in Eq. 23.
321 $$m_{CO_2} = MW_{CO_2} \times C_T \times V \quad (23)$$

Having m_{CO_2} and time (t), the transfer rate of CO_2 (J_{CO_2}) into the solution was then computed in units of g-CO_2 m^{-2} of fibers per unit time using Eq. 24. The surface area (SA) of the membrane module was computed using Eq. 25, which is based on the diameter of the HFM (D, m), the length of one fiber (l, m), and the number of fibers used (n). The change in concentration of DIC over time could be calculated using Eq. 26. The concentration of DIC present in the solution at $t = 0$ ($C_{T,0}$) was 0.005 M.

$$J_{CO_2} = \frac{(m_{CO_2})_{i+\Delta t} - (m_{CO_2})_i}{SA \times \Delta t} \quad (24)$$

$$SA = \pi n l D \quad (25)$$

$$N_{CO_2} = \frac{(m_{CO_2})_{i+\Delta t} - (m_{CO_2})_i}{V \times \Delta t} \quad (26)$$

Table 1 states the values for the constant parameters used in the model.

Table 1. Values of the constants in the model

Parameter	Symbol	Value	Units	Reference
Ionic product of water	K_W	10^{-14}	$mol^2\ dm^{-6}$	[19]
Hydration equilibrium	K	0.0016	–	[19]
First dissociation constant	K_1	6.3	–	[11]
Second dissociation constant	K_2	10.3	–	[11]
Henry's law constant	H^{cp}	0.336	$mol\ m^{-3}\ kPa^{-1}$	[21]
Reactor volume	V	0.7	L	Experimental
Carbon dioxide molecular weight	MW_{CO_2}	44	$g\ mol^{-1}$	–

335 Having C_T and N_{CO_2}, K_La was computed using the mass balance in Eqs. 1 and 26.

336 $$K_La = \frac{N_{CO_2}}{C^*_{CO_{2(aq)}} - C_{CO_{2(aq)}}} \quad (27)$$

337 K_L was then calculated from:

338 $$K_L = \frac{J_{CO_2}}{\Delta C} \quad (28)$$

339 The effective gas-liquid interfacial area per unit volume (a) was then computed from Eq. 29.

340 $$a = \frac{K_La}{K_L} \quad (29)$$

341

342 ## 3. Results and Discussion

343 ### 3.1. Model Accuracy

344 Figure 2 presents the results for the experiment in which the DIC concentration was
345 measured in parallel to the pH measurements to evaluate the accuracy of the model. The model-
346 predicted DIC concentrations matched the measured DIC values for pH values down to
347 approximately 7.5, when the experimental data deviated from the predicted DIC concentrations.
348 At low pH, the solution was super-saturated with CO_2 compared to its concentration in
349 equilibrium with atmospheric carbon dioxide (~400 ppm), and some CO_2 off-gassed before the
350 sample could be analyzed. The solution could absorb CO_2 from the atmosphere at very high pH
351 to approach equilibrium with atmospheric CO_2, but the result in Figure 2 does not indicate
352 significant absorption. To ensure that CO_2 off-gassing or absorption were not affecting the
353 analyses, the pH range for computing C_T and K_La was restricted to 10 to 8, where model-
354 predicted DIC values definitely were accurate.

355

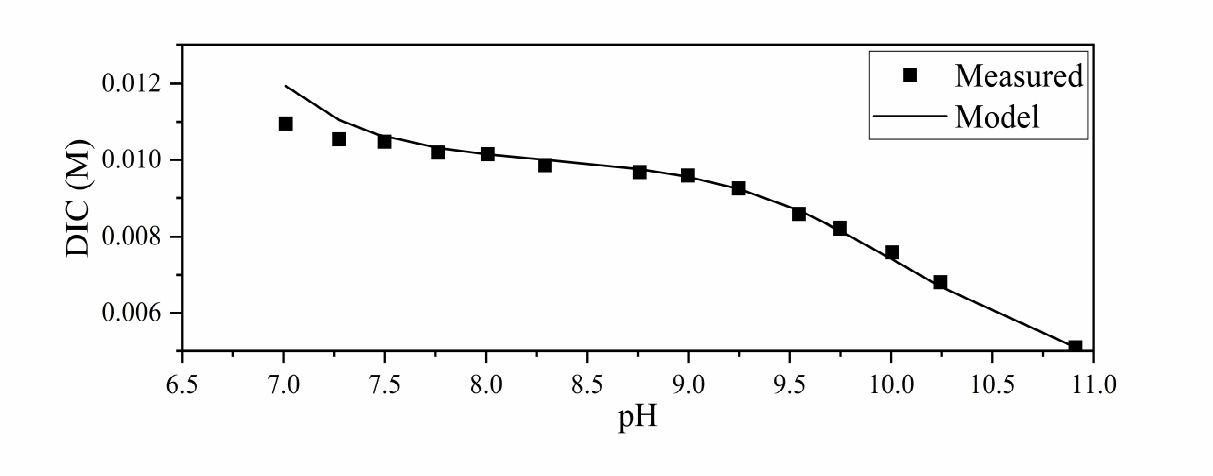

356

357 **Figure 2.** Comparison of DIC concentrations computed by the model versus measured values
358 using open-end HFM modules of 32 fibers of 0.18 m in length, supplied with 90%
359 CO_2, and diluting samples with non-acidified DI water.

360

361 **3.2. Open- vs Closed-End Fibers**

362 Table 2 compares the model-computed and directly measured CO_2 fluxes for open versus
363 closed HFMs supplied with 90% CO_2. The membrane-module configuration using 32 fibers,
364 0.18 m in length, was used to produce the results shown in Figure 2 and Table 2. Again,
365 measured and computed fluxes were nearly the same. The most important trend is that the CO_2
366 flux was about 3-fold greater for the open-end fibers. This difference was caused by the buildup
367 of inert gases (N_2, O_2, and H_2O vapor) with closed-end operation, which caused the CO_2
368 concentration to decrease along the fiber lumen away from the source of gas supply. As a result,
369 the distal end of the membrane lumen lost the capacity to transfer CO_2 to the liquid. In contrast,
370 an open-end fiber did not have a buildup of inert gases, since the inert gases were vented out.
371 The disadvantage of an open-end module is that high CO_2-transfer efficiency can be low because
372 a large amount of CO_2 is vented.

Table 2. Comparison of model-computed and directly measured DIC-based carbon dioxide fluxes between pH 10 – 8 for a module consisting of 32 fibers, 0.18 m in length operated in open-end mode and closed-end mode, supplied with 90% CO_2 at 69 kPa-gauge.

Operating Condition	pH 10 – 8 Flux ($g\ m^{-2}\ day^{-1}$)	
	Measured	**Predicted**
Open-end	2200	2000
Closed-end	590	640

The pressure dependence of CO_2 flux is shown in Figure 3a for open-end and closed-end fibers supplied with either 100% or 50% CO_2. For 100% CO_2, higher CO_2 partial pressure clearly increased the driving force for mass transfer in a roughly linear manner, and the open-end fibers had lower CO_2 fluxes for all but the lowest pressure. The open-end HFM had lower CO_2 flux for 100% CO_2 because it experienced a large pressure drop across the membrane's length: the pressure of the effluent gas was close to atmospheric pressure, or 0 kPa-gauge, which means that the average gas pressure inside the lumen was approximately 34.5 kPa-gauge. Figure 3b plots the fluxes versus the average total gas pressure. For 100% CO_2, the linear proportionalities between CO_2 flux and CO_2 pressure were nearly identical (~ 33 $g\ m^{-2}\ day^{-1}\ kPa^{-1}$) when the average pressure was taken into account.

The fluxes with 50% CO_2 were substantially lower than for 100% CO_2 and did not increase significantly with gas pressure for closed-end and open-end HFMs. The decrease in flux, compared to 100% CO_2, was much larger for closed-end operation, because the buildup of inert gases became the dominant effect, leading to lower flux across the membrane wall. In fact,

393 the effect of inert-gas accumulation in the closed-end mode affected flux to such a large degree
394 that the closed-end flux was much smaller even though the lumen in the open-end mode
395 experienced a large pressure drop, which is accounted for in Figure 3b. The lack of sensitivity to
396 inlet pressure probably was due to added mass-transfer resistance caused by the buildup of inert
397 gases in the fiber's lumen; the inert gases created a diffusion layer for CO_2 within the lumen.
398
399

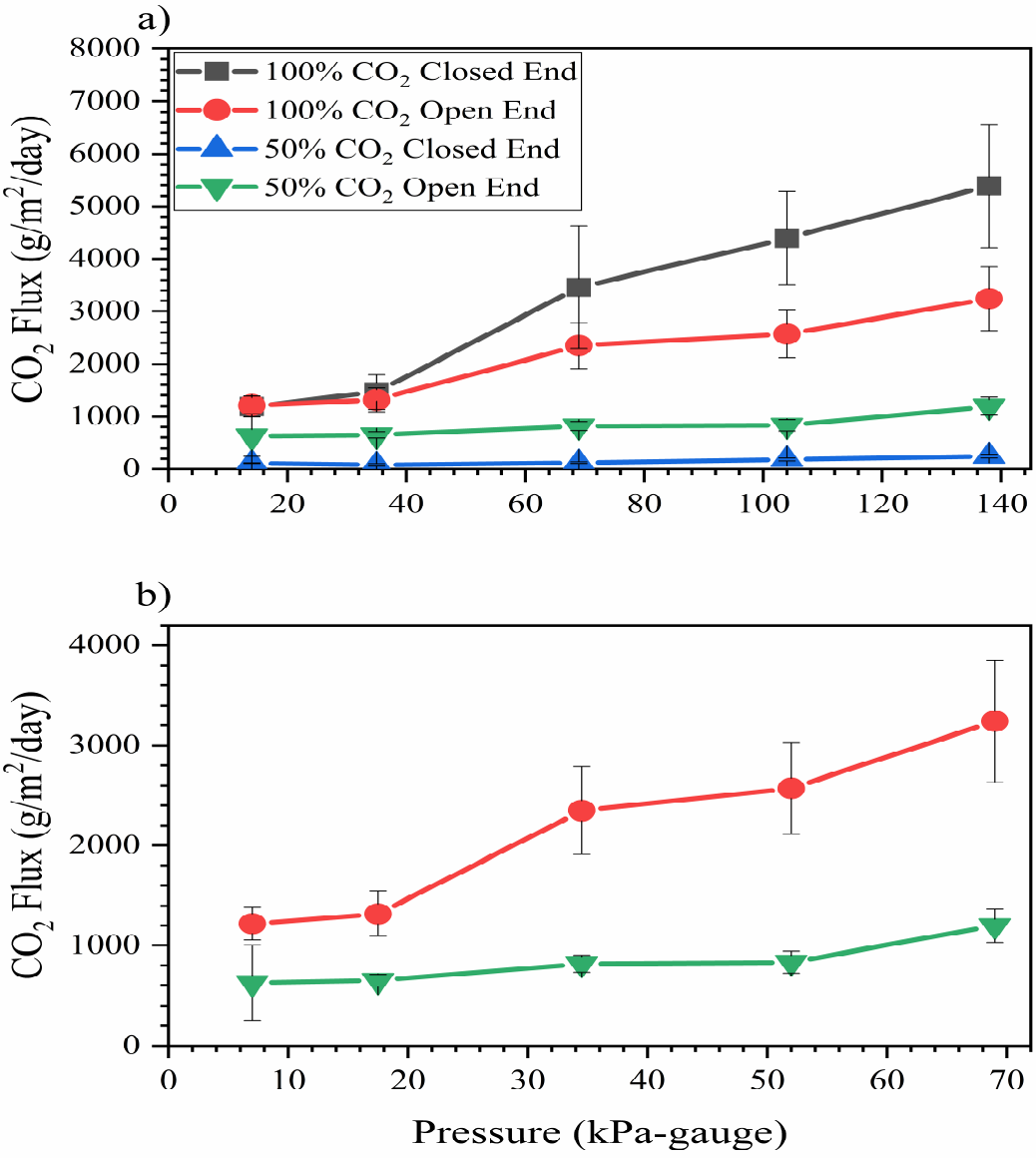

400

401 **Figure 3.** Pressure dependence of CO_2 flux for open-end or closed-end membrane modules
402 consisting of 96 fibers, 0.21 m in length based on a) total gas inlet pressure for
403 closed-end and open-end operation, and b) average total gas pressure across the
404 lumen for open-end operation. Error bars represent the standard deviation of the CO_2
405 fluxes computed by the model from the data along the time course of each
406 experiment.

3.3. CO_2 Partial Pressure

The effect of the CO_2 concentration in the inlet gas on HFM transfer rates is shown in Figure 4. Consistent with Figure 2 and Table 2, the membrane module used here consists of 32 fibers, 0.18 m in length. As expected, the CO_2 flux decreased as the concentration of CO_2 in the inlet stream decreased. For CO_2-enriched air (i.e., $\leq$90% CO_2), an open-end HFM performed better than a closed-end HFM, due to the accumulation of inert gases in the fiber lumen in the closed-end mode; inert gases were vented out the distal end of the fiber in the open-end mode. For pure CO_2, the performance of the closed-end module was greatly improved and similar to that of open-end mode, suggesting that the accumulation of inert gases was not significant with 100% CO_2.

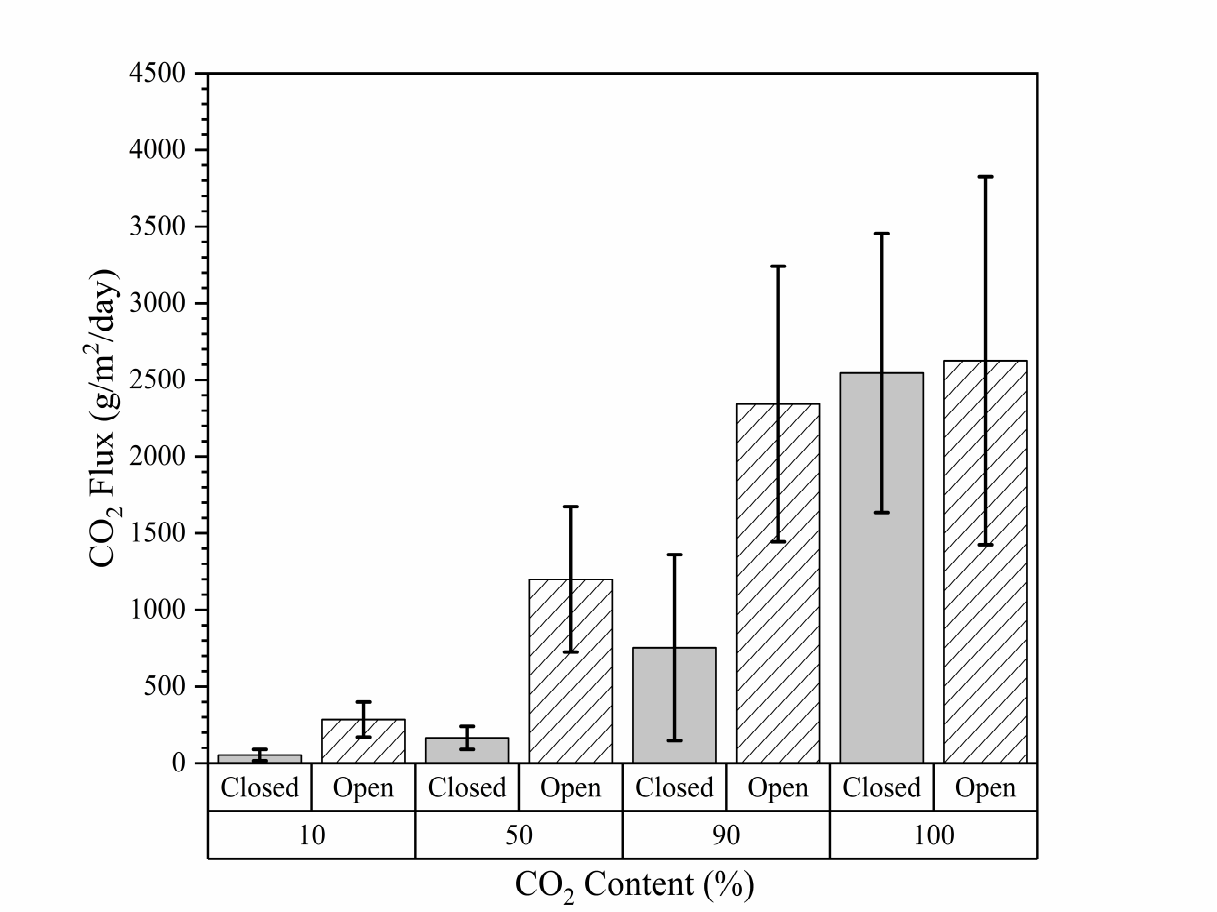

Figure 4. Effect of inlet CO_2 composition on flux evaluated for an inlet gas pressure of 69 kPa-gauge; however, the average gas pressure at the outlet of the lumen was 69 kPa and 34.5 kPa for closed-end and open-end mode, respectively. Data presented are the average of three HFM modules consisting of 32 fibers, varying from 13 cm to 18 cm in length. Error bars represent the standard deviation of data.

In Figure 4, the open-end and closed-end fluxes are almost equal for pure CO_2, which differs from the trends shown in Figure 3. The difference occurs because Figure 4 shows data only for 32-fiber membrane modules, while Figure 3 shows data only for a 96-fiber membrane module. The potting method used to assemble the membrane modules affected CO_2 flux, as

shown in Table 3. Modules consisting of 96 fibers and 64 fibers were potted using urethane adhesive, which required cutting uncoated fibers and led to pinching of some fibers, resulting in lower fluxes. An improvement was made for modules containing 32 fibers, which were potted using liquid resin to encase fibers prior to cutting and did not experience pinching.

Table 3. Comparison of fluxes for different potting methods and fiber lengths. Membrane modules consisting of 96 fibers, 21 cm in length, and 64 fibers, 39 cm in length, both potted using urethane adhesive. Membrane modules consisting of 32 fibers, 18 cm in length potted using liquid resin.

Operating Condition	**CO_2 Content (%)**	**Flux ($g\ m^{-2}\ day^{-1}$)**		
		96 fibers, 0.21 m	**64 fibers, 0.39 m**	**32 fibers, 0.18 m**
Open-end	100	3460	–	2550
Closed-end	100	2350	–	2630
Open-end	90	1060	590	2150
Closed-end	50	48	–	165
Open-end	50	445	360	1200

3.4. Mass-Transfer Coefficients and Effective Surface Areas

The values of overall volumetric mass-transfer coefficient (K_La), overall mass-transfer coefficient (K_L), and the interfacial area per unit reactor volume (a) for the composite HFM are shown in Table 4 for 100% CO_2. K_La and K_L were measured directly from the mass-transfer experiments using Eqs. 27 and 28, and then a was calculated using Eq. 29. The average K_L for the composite HFM, based on all values in Table 4, was $(5.37 \pm 0.01) \times 10^{-2}$ m hr^{-1}, and it was $(6.23 \pm 0.01) \times 10^{-2}$ m hr^{-1} for the open-end experiments. This difference supports that the

buildup of inert gases in closed-end operation lowered the effective membrane area below the maximum membrane area available for mass transfer. Thus, the loss of CO_2-transfer rate can be represented by a decrease in the effective surface area active in CO_2 delivery. Taking the ratio of K_La values, the effective a for closed-end operation was about 86% of the total for these experiments.

As shown in Table 4, K_La increased with fiber length, because a larger membrane surface area was available for mass transfer, as evidenced by increasing a values.

Table 4. Mass transfer coefficient and interfacial area values for 32-fiber HFM modules supplied with pure CO_2 at 69 kPa-gauge.

Operating Condition	No. of Fibers	Fiber Length (m)	K_La (hr^{-1})	$K_L \times 10^2$ ($m\ hr^{-1}$)	a (m^{-1})
Open-end	32	0.13	0.330	6.30	5.23
Open-end	32	0.17	0.471	6.88	6.84
Open-end	32	0.18	0.410	5.65	7.24
Closed-end	32	0.13	0.239	4.58	5.23
Closed-end	32	0.17	0.306	4.47	6.84
Closed-end	32	0.18	0.314	4.34	7.24

Note: K_La and K_L were measured experimentally, and a is the geometric surface area computed as $(K_La)/K_L$.

Table 5 summarizes the experimental K_La values and effective a values using $K_L = 6.23 \times 10^{-2}$ m hr^{-1}, from Table 4. The maximum utilizable a for the membranes in these experiments was 7.24 m^{-1}. The effective fiber length used was calculated from Eq. 25 based on the ratio of the effective a to the maximum a. The effective a and usable fiber lengths were substantially lower for closed-end mode than open-end mode, due to the buildup of inert gases, which decreased the surface area able to transfer CO_2 to the liquid. Decreasing the CO_2 concentration

469 in the supply gas amplified the impact of inert gases on the values for effective *a* and fiber
470 length.

471 It is possible that packing density could have affected the K_L and K_La values by affecting
472 the flow distribution through and around the fibers. However, Figure 5 illustrates that the fibers
473 were loosely packed in the reactor, and mixing from the stirrer was strong. Thus, the impact of
474 membrane packing density on CO_2 flux probably was low. Most importantly, any impact of
475 packing density would have had no effect on the measurement of pH and computation of the CO_2
476 flux.

477

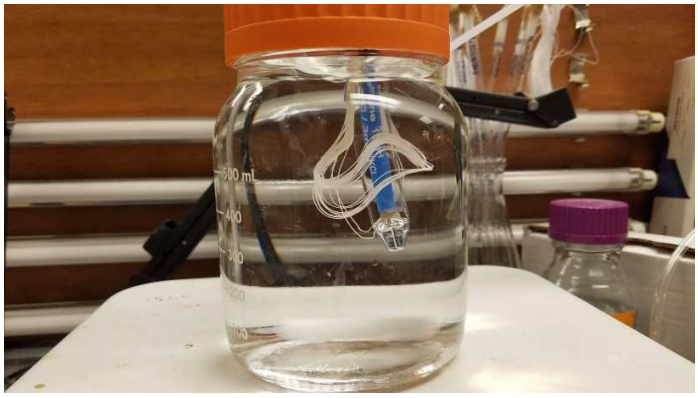

478

479 **Figure 5.** CO_2 delivery with HFM membrane.

480

481

Table 5. CO_2-transfer and HFM characteristics were affected by CO_2 inlet concentration and open-end versus closed-end operation. The modules consisted of 32 fibers, 0.18 m in length, and supplied with gas at 69 kPa-gauge.

CO_2 Content (%)	**Operating Condition**	**Flux ($g\ m^{-2}\ day^{-1}$)**	**K_La (hr^{-1})**	**Effective a (m^{-1})**	**Usable Fiber Length (m)**	**(%)**
90	Open	2150	0.372	5.97	0.15	83
50	Open	1200	0.374	6.00	0.15	83
10	Open	200	0.294	4.72	0.12	65
90	Closed	750	0.103	1.65	0.04	23
50	Closed	165	0.041	0.66	0.02	10
10	Closed	53	0.041	0.66	0.02	10

4. Conclusion

A model was developed to estimate mass-transfer coefficients and CO_2-transfer rates for a composite HFM based on the measured rate of change of pH. The model accurately calculated transfer rates between a pH range of 10 to 8. CO_2-transfer rates and K_La values increased with increasing inlet gas pressure and increasing CO_2 concentrations in the inlet gas stream. Open-ended modules tested with pure CO_2 exhibited the highest flux and K_L values. Closed-ended modules performed nearly as well as open-ended modules when supplied with pure CO_2; however, the performance of closed-ended modules significantly dropped off as the concentration of inert gases in the supply stream was increased. A decrease in the usable membrane surface area (a) also followed the same trend due to the accumulation of inert gases in the membrane lumen.

5. Acknowledgments

This work was supported by the Department of Energy Office of Energy Efficiency and Renewable Energy, Bioenergy Technology Office award number DE-EE0007093. The authors would also like to thank Megha Patel and Binh Nguyen for their insights into this work.

6. References

[1] R. Davis, A. Aden, P.T. Pienkos, Techno-economic analysis of autotrophic microalgae for fuel production, Appl. Energy. 88 (2011) 3524–3531. doi:10.1016/j.apenergy.2011.04.018.

[2] D.W. Keith, G. Holmes, D. St. Angelo, K. Heidel, A Process for Capturing CO 2 from the Atmosphere, Joule. 0 (2018). doi:10.1016/j.joule.2018.05.006.

[3] K.S. Lackner, The thermodynamics of direct air capture of carbon dioxide, Energy. 50 (2013) 38–46. doi:10.1016/j.energy.2012.09.012.

[4] H.W. Kim, A.K. Marcus, J.H. Shin, B.E. Rittmann, Advanced Control for Photoautotrophic Growth and CO2-Utilization Efficiency Using a Membrane Carbonation Photobioreactor (MCPBR), Environ. Sci. Technol. 45 (2011) 5032–5038. doi:10.1021/es104235v.

[5] Y.K. Lee, H.K. Hing, Supplying CO2 to photosynthetic algal cultures by diffusion through gas-permeable membranes, Appl. Microbiol. Biotechnol. 31 (1989) 298–301.

[6] A.P. Carvalho, F.X. Malcata, Transfer of carbon dioxide within cultures of microalgae: Plain bubbling versus hollow-fiber modules, Biotechnol. Prog. 17 (2001) 265–272. doi:10.1021/bp000157v.

[7] M.A. Voss, T. Ahmed, M.J. Semmens, Long-term performance of parallel-flow, bubbleless, hollow-fiber-membrane aerators, Water Environ. Res. 71 (1999) 23–30. doi:10.2175/106143099x121616.

[8] T. Ahmed, M.J. Semmens, Use of sealed end hollow fibers for bubbleless membrane aeration - Experimental studies, J. Memb. Sci. 69 (1992) 1–10. doi:10.1016/0376-7388(92)80162-d.

[9] T. Ahmed, M.J. Semmens, The use of independently sealed microporous hollow fiber membranes for oxygenation of water - Model development, J. Memb. Sci. 69 (1992) 11–20. doi:10.1016/0376-7388(92)80163-e.

[10] R. Putt, M. Singh, S. Chinnasamy, K.C. Das, An efficient system for carbonation of high-rate algae pond water to enhance CO2 mass transfer, Bioresour. Technol. 102 (2011) 3240–3245. doi:10.1016/j.biortech.2010.11.029.

[11] W. Stumm, J.J. Morgan, Aquatic chemistry: chemical equilibria and rates in natural waters, 3rd ed.., 1996.

[12] B. Wang, Y.Q. Li, N. Wu, C.Q. Lan, CO2 bio-mitigation using microalgae, Appl. Microbiol. Biotechnol. 79 (2008) 707–718. doi:10.1007/s00253-008-1518-y.

[13] A. Kumar, S. Ergas, X. Yuan, A. Sahu, Q. Zhang, J. Dewulf, F.X. Malcata, H. van Langenhove, Enhanced CO2 fixation and biofuel production via microalgae: recent developments and future directions, Trends Biotechnol. (2010). doi:10.1016/j.tibtech.2010.04.004.

[14] P. Perez-Calleja, M. Aybar, C. Picioreanu, A.L. Esteban-Garcia, K.J. Martin, R. Nerenberg, Periodic venting of MABR lumen allows high removal rates and high gas-transfer efficiencies, Water Res. 121 (2017) 349–360. doi:10.1016/j.watres.2017.05.042.

[15] T. Ahmed, M.J. Semmens, Use of transverse flow hollow fibers for bubbleless membrane aeration, Water Res. 30 (1996) 440–446. doi:10.1016/0043-1354(95)00167-0.

[16] A.F. Ismail, S.N. Kumari, Potential effect of potting resin on the performance of hollow fibre membrane modules in a CO 2 / CH 4 gas separation system, 236 (2004) 183–191. doi:10.1016/j.memsci.2004.02.023.

[17] T.G. Skog, S. Johansen, M.B. Hägg, Method to prepare lab-sized hollow fiber modules for

gas separation testing, Ind. Eng. Chem. Res. (2014). doi:10.1021/ie4041059.

[18] A.P. Carvalho, L.A. Meireles, F.X. Malcata, Microalgal Reactors: A Review of Enclosed System Designs and Performances, Biotechnol. Prog. 22 (2006) 1490–1506. doi:10.1021/bp060065r.

[19] S.K. Lower, Carbonate equilibria in natural waters, Chem1 Virtual Textb. (1999) 1–26. http://www.chem1.com/acad/webtext/pdf/c3carb.pdf.

[20] G.A. Hill, Measurement of Overall Volumetric Mass Transfer Coefficients for Carbon Dioxide in a Well-Mixed Reactor Using a pH Probe, Ind. Eng. Chem. Res. 45 (2006) 5796–5800. doi:10.1021/IE060242T.

[21] R. Sander, Compilation of Henry's law constants (version 4.0) for water as solvent, Atmos. Chem. Phys. 15 (2015) 4399–4981. doi:10.5194/acp-15-4399-2015.

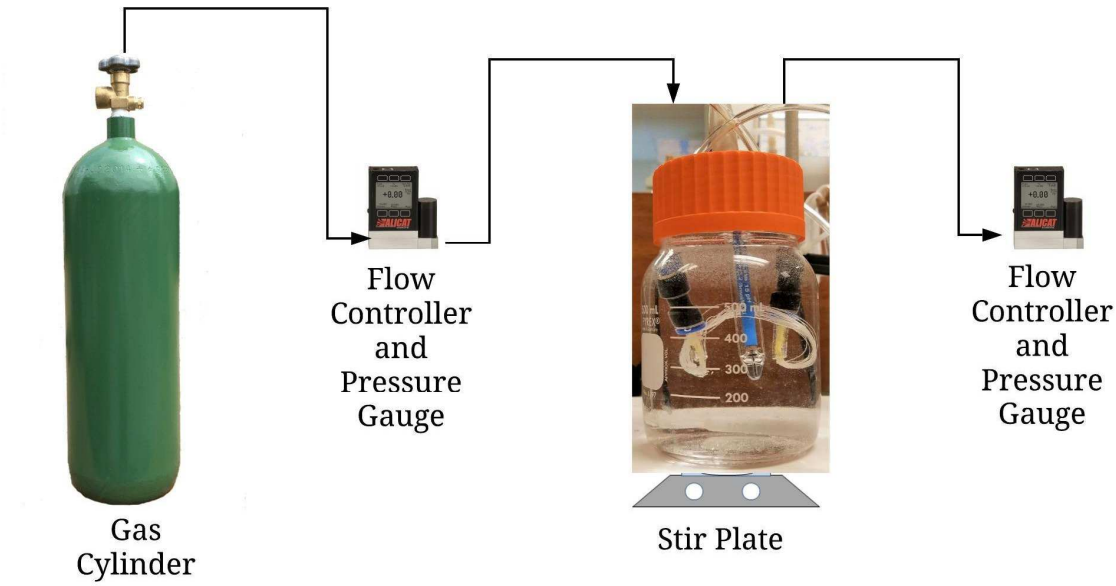

Figure 1. Experimental setup used for abiotic testing.

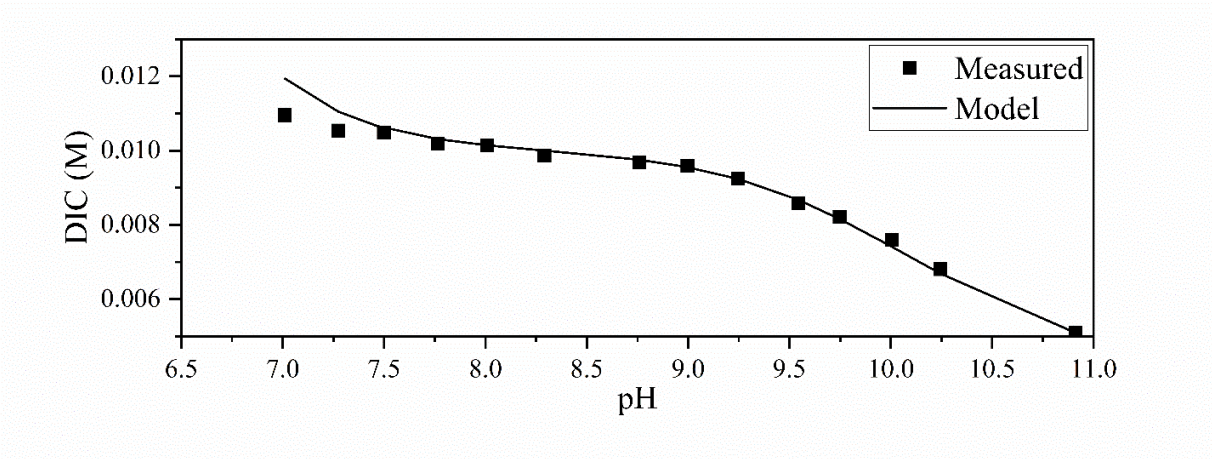

Figure 2. Comparison of DIC concentrations computed by the model versus measured values using open-end HFM modules of 32 fibers of 0.18 m in length, supplied with 90% CO_2, and diluting samples with non-acidified DI water.

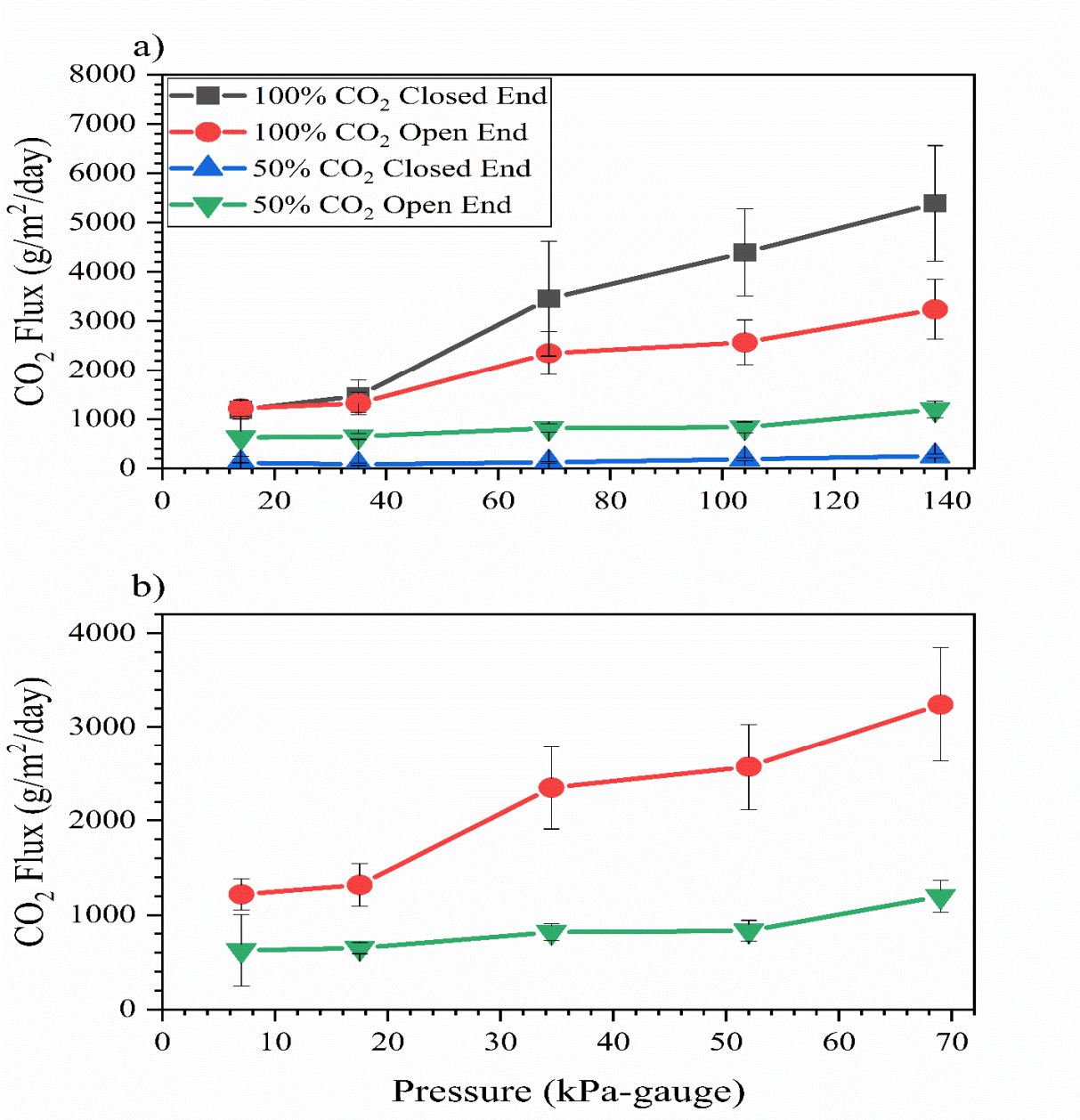

Figure 3. Pressure dependence of CO_2 flux for open-end or closed-end membrane modules consisting of 96 fibers, 0.21 m in length based on a) total gas inlet pressure for closed-end and open-end operation, and b) average total gas pressure across the lumen for open-end operation. Error bars represent the standard deviation of the CO_2 fluxes computed by the model from the data along the time course of each experiment.

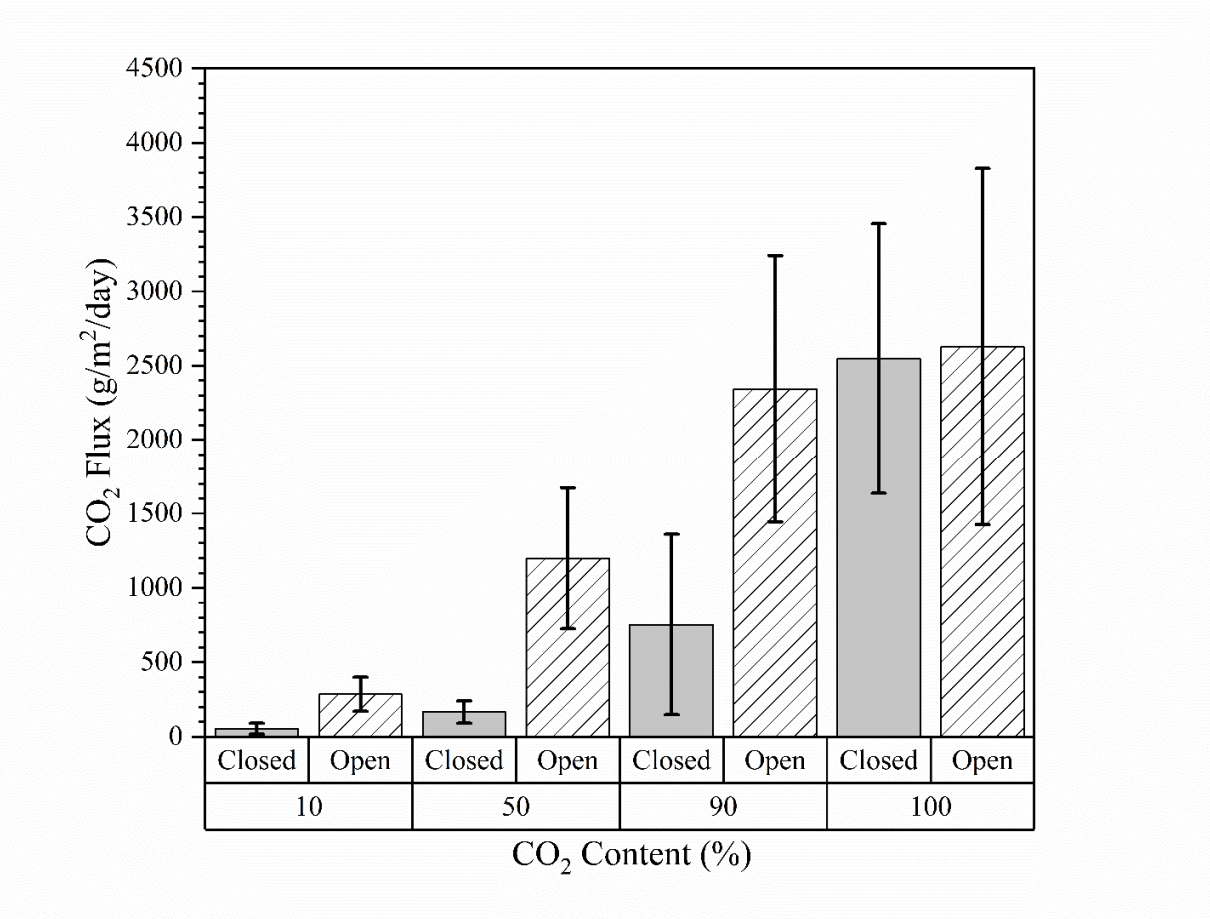

Figure 4. Effect of inlet CO_2 composition on flux evaluated for an inlet gas pressure of 69 kPa-gauge; however, the average gas pressure at the outlet of the lumen was 69 kPa and 34.5 kPa for closed-end and open-end mode, respectively. Data presented are the average of three HFM modules consisting of 32 fibers, varying from 13 cm to 18 cm in length. Error bars represent the standard deviation of data.

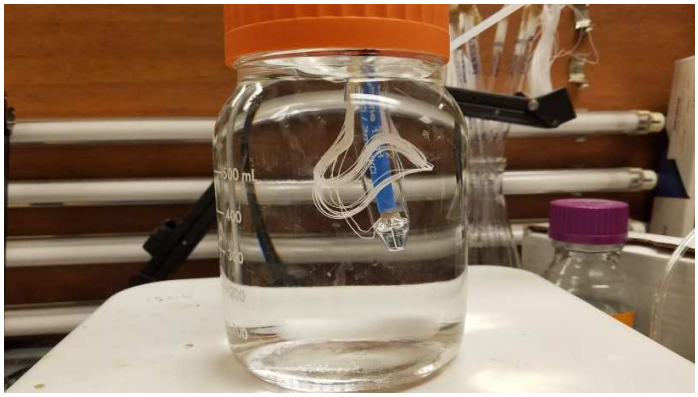

Figure 5. CO_2 delivery with HFM membrane.